High spin spectroscopy and shears mechanism in ^{107}In

D. Negi,[1,*] T. Trivedi,[2] A. Dhal,[1,8] S. Kumar,[3] V. Kumar,[3] S. Roy,[4] M. K. Raju,[5] S. Appannababu,[6] G. Mohanto,[1] J. Kaur,[7] R. K. Sinha,[8] R. Kumar,[1] R. P. Singh,[1] S. Muralithar,[1] A. K. Bhati,[7] S. C. Pancholi,[1,3] and R. K. Bhowmik[1]

[1]*Inter University Accelerator Centre, Aruna Asaf Ali Marg, New Delhi 110067, India*
[2]*Department of Physics, University of Allahabad, Allahabad 211002, India*
[3]*Department of Physics and Astrophysics, University of Delhi, Delhi 110007, India*
[4]*S.N. Bose National Centre for Basic Sciences, Block JD, Sector III, Kolkata 700098, India*
[5]*Department of Nuclear Physics, Andhra University, Visakhapatnam 530003, India*
[6]*Department of Physics, M.S. University of Baroda, Vadodara 390002, India*
[7]*Department of Physics, Punjab University, Chandigarh 160014, India*
[8]*Department of Physics, Banaras Hindu University, Varanasi 221005, India*

(Received 10 February 2010; revised manuscript received 17 April 2010; published 28 May 2010)

High spin states of ^{107}In have been investigated using the reaction ^{94}Mo(^{16}O, $p2n$)^{107}In at a beam energy of 70 MeV. A total of 62 new γ transitions have been placed in the level scheme and several $\Delta I = 1$ sequences and one $\Delta I = 2$ sequence have been found. Lifetime measurements using the Doppler-shift attenuation method (DSAM) have been carried out for band states of $\Delta I = 1$ and $\Delta I = 2$. A decreasing trend of $B(M1)$ strengths with increasing spin deduced for the $\Delta I = 1$ band indicates the presence of a shears mechanism. The experimental data for this band are compared with the tilted axis cranking (TAC) calculations. The $\Delta I = 2$ band has been found to be a deformed band with $\beta_2 \sim 0.2$.

DOI: 10.1103/PhysRevC.81.054322 PACS number(s): 21.10.Hw, 21.10.Tg, 23.20.−g, 27.60.+j

I. INTRODUCTION

Nuclei in the $A \sim 110$ region are host for many interesting phenomenon. Being in the close vicinity of the $Z = 50$ shell closure, their low spin states are generated predominantly by single-particle excitations. However, at high spins there are other possible excitation mechanisms present. One such mode of excitation is the "shears mechanism," which is explained within the framework of the tilted axis cranking (TAC) model [1]. In this case, sequences of $M1$ γ transitions are observed with weak or missing crossover $E2$ transitions, indicating small deformation of the structures involved. These $M1$ transitions have highly reduced $B(M1)$ strengths and the ratio of the dynamic moment of inertia to the reduced $B(E2)$ strength is large [$>100\hbar^2$ MeV^{-1} (e b)$^{-2}$]. In nuclei with $Z < 50$ and $N > 50$ the bandhead configuration of these sequences results from the near-perpendicular coupling of angular momentum vectors of high-Ω $g_{9/2}$ proton holes $\mathbf{j}_\pi$ with low-Ω neutron particles $\mathbf{j}_\nu$ in $h_{11/2}$, $g_{7/2}$, and/or $d_{5/2}$ orbitals. As a result of near-perpendicular coupling, the resulting total angular momentum vector $\mathbf{I}$ makes an angle ϑ with the symmetry axis of the slightly deformed core. Further angular momentum generation along the band takes place by the gradual alignment of $\mathbf{j}_\pi$ and $\mathbf{j}_\nu$ toward the total angular momentum vector $\mathbf{I}$. With this gradual alignment, the perpendicular component of the magnetic moment $\mu_\perp$ decreases with increasing spin, which is reflected as a decrease of $B(M1)$ values along the band and serve as an important criterion for the presence of the shears mechanism in the band.

It is of particular interest to investigate the shears mechanism along an isotopic chain in this region. With change in neutron number a gradual change in quadrupole deformation is explicit. This helps in understanding the relative contribution of core and shears mechanism in spin generation along a band for the same set of active quasiparticles. At low deformation where the contribution of the core is significantly less and the competition from single-particle excitations is higher, the shears mechanism disappears and leads into irregular spaced shell-model states. A study for the determination of the lower boundary of the shears mechanism in Ag isotopes has been carried out in Ref. [2]. In odd-In isotopes the shears mechanism has been observed only in the heavier indium isotopes ^{111,113}In [3], whereas in even-In isotopes it has been observed down to ^{106}In [4]. Although several $\Delta I = 1$ sequences have been observed in lighter odd-A indium isotopes ($A < 109$) [5], the $B(M1)$ strengths for these states are not known. Of particular interest is a sequence of states labeled as band 1 in ^{105,107}In [5]. Although low spin states in these nuclei have been explained successfully by the hole-core coupling model, with neighboring Sn nuclei as a core [6], the explanation of these $\Delta I = 1$ states was not so successful. Shell-model calculations have also been carried out for these sequences [5,7]. The agreement between the calculations and the experimental results are better for the level excitation energies but the $B(M1)$ strengths measured for a few states in ^{105}In fail to agree with calculations [7]. These observations indicate that a different excitation mechanism other than single-particle excitation is responsible for the generation of spin in these sequences. The measurement of $B(M1)$ strengths of these states will help to shed more light on their structure.

The present study is aimed at the investigation of $\Delta I = 1$ negative-parity bands in ^{107}In. In previous investigations of ^{107}In [5,8] two $\Delta I = 1$ bands were established. In this work the level scheme of ^{107}In has been significantly extended with the observation of several $\Delta I = 1$ bands and a $\Delta I = 2$ band.

*din_physics@yahoo.co.in

Lifetime measurements have also been performed for a $\Delta I = 1$ band and the $\Delta I = 2$ band.

While this manuscript was under preparation, a paper on ^{107}In was published [9]. Similarities and differences with their work [9] and a very recent work [10] are also discussed in the present paper.

II. EXPERIMENTAL DETAILS AND DATA ANALYSIS

In the present experiment high spin states of ^{107}In were populated using the reaction ^{94}Mo(^{16}O, $p2n$)^{107}In at a beam energy of 70 MeV delivered by the 15UD Pelletron Accelerator at the Inter University Accelerator Centre (IUAC), New Delhi [11,12]. The γ rays emitted in the reaction were detected by the Indian National Gamma Array (INGA) [13,14], which at the time of the experiment comprised seventeen Compton-suppressed Ge clover detectors with three at 32°, three at 57°, five at 90°, two at 123°, and four at 148° with respect to the beam axis. An isotopically enriched ^{94}Mo target of thickness 0.9 mg/cm^2 with 6.5 mg/cm^2 thick ^{197}Au backing was used. The collection of data was done in the list mode format using the CAMAC-based multicrate synchronization mode on a Linux platform. The in-house software CANDLE [15] was used for this purpose. The trigger for data collection was set in the γ-γ mode. A total of one-billion γ-γ events were recorded.

The data were sorted using the INGASORT [16] program. After matching the gain of the initial energy spectra to 0.5 keV per channel, different 4k × 4k matrices were constructed. The symmetrized matrix compatible with the RADWARE format was used in the RADWARE program [17] for coincidence analysis. Additionally, the γ-γ-γ events that were collected along with the γ-γ events were used to form a γ-gated matrix with a gate on strong transitions of ^{107}In. Since the energy axis in the γ-gated matrix is not compressed, the spectrum obtained has a better resolution compared with the one obtained from the double-γ-gated projection of CUBE (RADWARE package [17]). This helps in better identification of new transitions. Wherever possible, intensities of higher lying transitions were obtained from double-gated spectra or their sums.

For directional correlation from oriented nuclei (DCO) analysis, four different asymmetric matrices were constructed with one axis corresponding to detectors at 90° and the other axis corresponding to detectors at one of the following angles: 32°, 57°, 153°, and 148°. The DCO ratios were calculated using the following relation:

$$R_{\mathrm{DCO}} = \frac{I^{\gamma_2}_{\theta_1}(\mathrm{Gate}^{\gamma_1}_{\theta_2})}{I^{\gamma_2}_{\theta_2}(\mathrm{Gate}^{\gamma_1}_{\theta_1})}. \tag{1}$$

The ratio is close to 1.0 for a quadrupole and 0.5 for a dipole transition when the gate is set on a quadrupole transition, under the assumption of pure and stretched character of all the transitions considered. However, a mixed $M1/E2$ transition, with a mixing ratio $\delta > 0$, can have a DCO ratio of 1.0. Hence, the DCO ratio of 1.0 is only a necessary condition and not sufficient for a stretched transition to be quadrupole in nature. This expression for the DCO ratio is integrated over the angle ϕ (the angle between the planes made by the two transitions with the beam axis [18]). Since the backed target was used in the experiment, a correction is made for the Doppler-shifted counts of the transitions from short-lived states while calculating the DCO ratios.

Linear polarization measurement of some of the transitions of ^{107}In was carried out using the integrated polarization directional correlation from oriented nuclei (IPDCO) method [19]. In this method, the polarization distribution of one of the coincident γ transitions is measured and the emission angle of a second coincident γ transition is integrated over 4π. This method is equivalent to the measurement of polarization distribution in singles with an essential difference of background reduction from the possibility of gating on other transitions of the nucleus. The polarization P of a γ transition is related to the experimental asymmetry Δ of the transition and the polarization sensitivity Q of the polarimeter by the relation $P = \Delta/Q$. For a Compton- polarimeter the experimental asymmetry Δ of the transition is defined by [19]

$$\Delta = \frac{aN_\perp - N_\parallel}{aN_\perp + N_\parallel}, \tag{2}$$

where $N_\perp(N_\parallel)$ is the number of counts of γ transitions scattered perpendicular (parallel) to the emission plane. The correction factor a in this relation is a measure of any asymmetry in the response of the perpendicular and the parallel detectors and was obtained from radioactive source data (^{152}Eu). It is defined as

$$a = \frac{N_\parallel(\mathrm{unpolarized})}{N_\perp(\mathrm{unpolarized})}. \tag{3}$$

The value of a for the 90° detectors of the array was found to have a nearly constant value of 0.99 over the energy range shown in Fig. 1.

In a clover detector one of the segments acts as a scatterer and the other as an analyzer. The polarization sensitivity Q of the clover as a function of photon energy is defined as $Q(E_\gamma) = Q_0(E_\gamma)(CE_\gamma + B)$ [19], where $Q_0(E_\gamma)$ is the

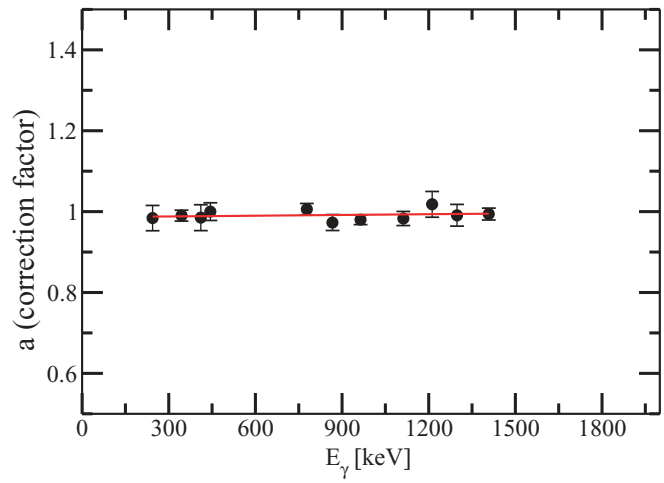

FIG. 1. (Color online) A plot of the correction factor a defined by Eq. (3) as a function of γ-ray energy. The results were obtained by summing the spectra of the 90° clover detectors of the INGA. The data points are from an unpolarized ^{152}Eu source. The value obtained is $a = 0.99$ and is nearly constant for the energy range 200 to 1500 keV.

polarization sensitivity of a point detector. The data for Q are taken from Ref. [20], where the measurements were carried out for a similar kind of setup using the clover detectors. For the analysis using the IPDCO method, two different asymmetric matrices with one axis corresponding to the detector at 90° and other axis corresponding to all the detectors of the array, were constructed. When the condition is set on the selection of events in which one of the coincident γ rays recorded by a clover detector at 90° undergoes scattering between the segments parallel to the orientation axis (here it is the beam axis), the matrix is called a parallel matrix. If the scattering is between the segments perpendicular to the orientation axis then the matrix is called a perpendicular matrix. Spectra made from these matrices by putting the gate on strong transitions of the nucleus were used to get the values of $N_\perp$ and $N_\parallel$ for a particular transition. The polarization of the transition was then obtained using Eq. (2).

III. RESULTS

A. Level scheme

The level scheme of ^{107}In deduced in the present work is based on γ-ray coincidence and intensity relationships and is shown in Fig. 2. Much of the level scheme of previous works [2,5] has been verified along with certain modifications and additions. The properties of transitions extracted in this work are listed in Table I. The γ-ray coincidence spectrum shown in Fig. 3 is obtained by setting a gate on the $17/2^+ \rightarrow 13/2^+$ (438-keV) transition in ^{107}In. The spins and parity of the ground state band from $9/2^+$ to $21/2^+$ levels have been adopted from Ref. [5]. The multipolarities determined in the present work for the 413-, 438-, 791-, 1002-, and 1415-keV transitions from the DCO ratio (except for the 438-keV transition) and polarization data are consistent with the above I^π assignment. A band referred to as "band 5" in Ref. [9] is not found in the present work. This is evidenced in the sum double-gated coincidence spectrum (Fig. 4), with the first gate on 316-, 360-, and 1533-keV transitions of band 2 and the second gate on the 438-keV transition ($17/2^+ \rightarrow 13/2^+$).

1. Band 1

Figure 5 shows the sum double-gated γ-ray coincidence spectrum for band 1. It has been extended at the top with the addition of 701-, 841-, and 589-keV transitions (see Fig. 2). The 589-keV transition is not visible in Fig. 5. Only when the gate was set on higher lying 383-, 504-, and 701-keV transitions was the 589-keV transition observed in the coincidence spectrum. The DCO ratio and polarization measurements of 1429- and 1438-keV decay transitions from the band confirm their $E1$ character. This firmly establishes the spins and the negative parity of the levels of the band at excitation energies of 3283 and 3442 keV. The in-band 383-, 393-, 532-, and 612-keV transitions were determined as $M1$ from the DCO ratio and polarization measurements. This confirms that the states of the band have negative parity. The 915-, 1005-, and 1144-keV crossover $E2$ transitions have also been observed. The crossover 363-keV ($23/2^- \rightarrow 21/2^-$) and 887-keV ($33/2^- \rightarrow 29/2^-$) transitions, mentioned in Ref. [9], were not observed in the gate of the 393-keV transition. The 597-keV transition was observed in the gate of all transitions of the band up to the 504-keV transition, including 393- and

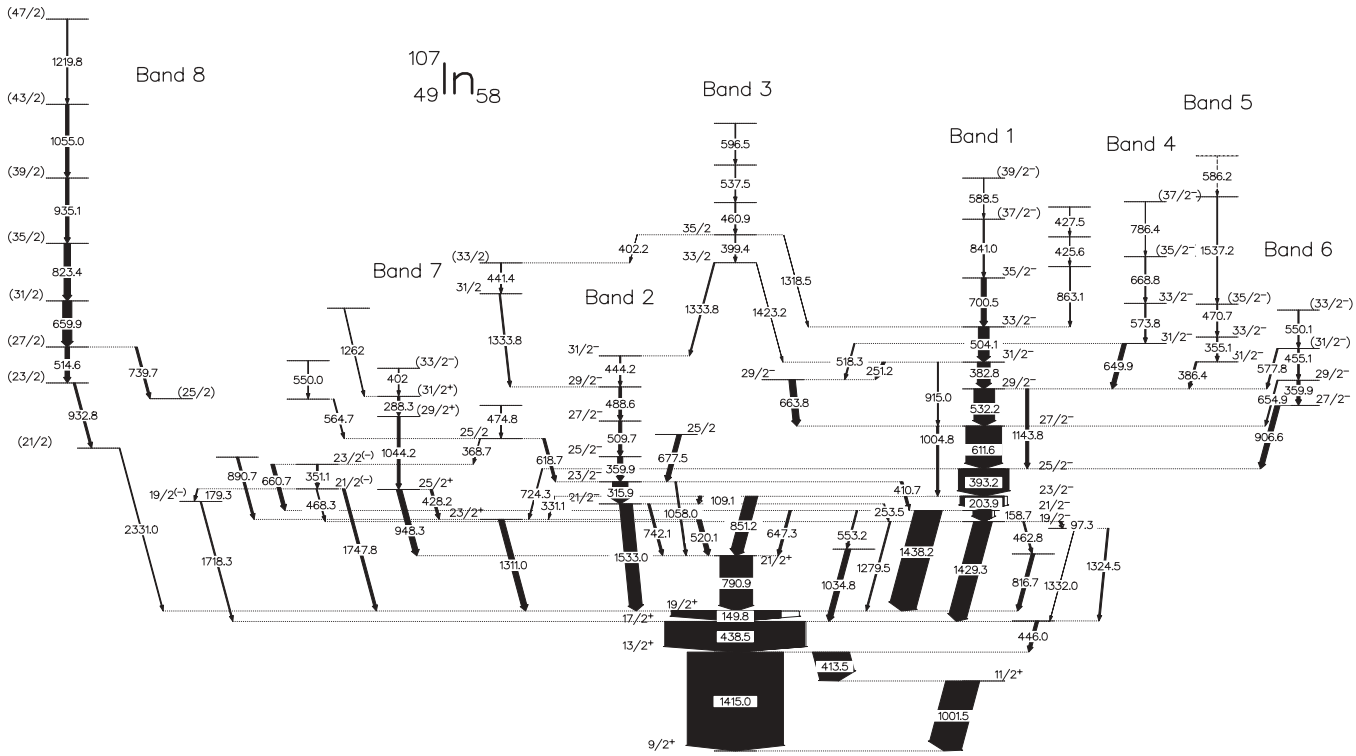

FIG. 2. Level scheme of ^{107}In deduced from the present data. The width of each arrow is proportional to the intensity of transition.

TABLE I. Energy, intensity, DCO ratio, multipolarity, IPDCO value, and initial and final state spin of the transitions of ^{107}In deduced from the present work. D stands for dipole and Q for quadrupole.

E_γ (keV)	E_x (keV)	I_γ	R_{DCO}(Q)	R_{DCO}(D)	Multipolarity	IPDCO	$J_i^\pi \rightarrow J_f^\pi$
97.3	3282.8	1.1(2)					$\frac{19}{2}^- \rightarrow$
109.1	3645.4	1.6(1)	0.95(17)	2.08(39)			$\frac{23}{2}^- \rightarrow \frac{21}{2}^-$
149.8	2003.3	78.6(7)	0.64(1)				$\frac{19}{2}^+ \rightarrow \frac{17}{2}^+$
158.7	3441.5	13.5(3)	0.63(2)		D		$\frac{21}{2}^- \rightarrow \frac{19}{2}^-$
179.3	3751.1	0.6(1)	0.64(15)		D		$\frac{21}{2}^{(-)} \rightarrow \frac{19}{2}^{(-)}$
203.9	3645.4	31.1(6)	0.59(2)		D		$\frac{23}{2}^- \rightarrow \frac{21}{2}^-$
251.2	5565.2	2.1(1)	0.55(8)		D		$\frac{31}{2}^- \rightarrow \frac{29}{2}^-$
253.5	3536.3	0.6(1)					$\frac{21}{2}^- \rightarrow \frac{19}{2}^-$
288.3	5075.0	1.6(2)	0.50(6)		D		$(\frac{31}{2}^+ \rightarrow \frac{29}{2}^+)$
315.9	3852.2	10.8(3)	0.58(2)		$M1$	−0.12(18)	$\frac{23}{2}^- \rightarrow \frac{21}{2}^-$
331.1	3645.4	0.3(1)					$\frac{23}{2}^- \rightarrow \frac{23}{2}^+$
351.1	4102.2	1.2(1)	0.51(6)		D		$\frac{23}{2}^{(-)} \rightarrow \frac{21}{2}^{(-)}$
355.1	5923.9	0.9(1)		0.82(12)	D		$\frac{33}{2}^- \rightarrow \frac{31}{2}^-$
359.9	4212.1	3.6(2)		1.01(8)	D		$\frac{25}{2}^- \rightarrow \frac{23}{2}^-$
359.9	5305.1	2.2(3)		1.00(11)	D		$\frac{29}{2}^- \rightarrow \frac{27}{2}^-$
368.7	4470.9	0.5(2)					$\frac{25}{2} \rightarrow \frac{23}{2}^{(-)}$
382.8	5565.2	9.0(3)		1.08(4)	$M1$	−0.06(12)	$\frac{31}{2}^- \rightarrow \frac{29}{2}^-$
386.4	5568.8	1.2(2)			$M1$	−0.12(33)	$\frac{31}{2}^- \rightarrow \frac{29}{2}^-$
393.2	4038.6	35.7(9)	0.58(1)		$M1$	−0.15(6)	$\frac{25}{2}^- \rightarrow \frac{23}{2}^-$
399.4	7387.8	0.6(1)	0.51(10)	0.90(20)	D		$\frac{35}{2} \rightarrow \frac{33}{2}$
402.0	5477.0	0.5(2)					$(\frac{33}{2}^+ \rightarrow \frac{31}{2}^+)$
402.2	7387.4	0.3(1)	0.38(13)	0.78(22)	D		$\frac{35}{2} \rightarrow (\frac{33}{2})$
410.7	3852.2	1.8(3)					$\frac{23}{2}^- \rightarrow \frac{21}{2}^-$
413.5	1415.0	28.0(11)	0.58(2)		$M1$	−0.15(15)	$\frac{13}{2}^+ \rightarrow \frac{11}{2}^+$
425.6	7358.0	0.4(2)					
427.5	7785.5	0.3(2)					
428.2	3742.5	1.7(2)					$\frac{25}{2}^+ \rightarrow \frac{23}{2}^+$
438.5	1853.5	100			$E2$	0.15(2)	$\frac{17}{2}^+ \rightarrow \frac{13}{2}^+$
441.4	6985.6	0.7(2)					$(\frac{33}{2}) \rightarrow \frac{31}{2}$
444.2	5654.6	0.8(1)		0.78(0.17)	D		$\frac{31}{2}^- \rightarrow \frac{29}{2}^-$
446.0	1861.0	2.3(3)					$\rightarrow \frac{13}{2}^+$
455.1	5760.2	1.1(1)					$(\frac{31}{2}^-) \rightarrow \frac{29}{2}^-$
460.9	7848.7	0.7(3)					$\rightarrow \frac{35}{2}$
462.8	3282.8	1.1(2)					$\frac{19}{2}^- \rightarrow$
468.3	3751.1	0.7(1)					$\frac{21}{2}^{(-)} \rightarrow \frac{19}{2}^-$
470.7	6394.6	0.7(2)					$(\frac{35}{2}^-) \rightarrow \frac{33}{2}^-$
474.8	4945.7	0.6(1)					$\rightarrow \frac{25}{2}$
488.6	5210.4	1.9(1)		0.98(18)	D		$\frac{29}{2}^- \rightarrow \frac{27}{2}^-$
504.1	6069.3	7.6(3)		1.09(11)	D		$\frac{33}{2}^- \rightarrow \frac{31}{2}^-$
509.7	4721.8	2.2(1)		0.90(14)	D		$\frac{27}{2}^- \rightarrow \frac{25}{2}^-$
514.6	5781.7	3.2(3)	0.88(15)		Q		$(\frac{27}{2} \rightarrow \frac{23}{2})$
518.3	5832.3	0.8(1)					$\frac{31}{2}^- \rightarrow \frac{29}{2}^-$
520.1	3314.3	3.2(2)					$\frac{23}{2}^+ \rightarrow \frac{21}{2}^+$
532.2	5182.4	14.7(5)	0.64(4)	0.98(5)	$M1$	−0.23(9)	$\frac{29}{2}^- \rightarrow \frac{27}{2}^-$

TABLE I. *(Continued.)*

E_γ (keV)	E_x (keV)	I_γ	$R_{\rm DCO}$(Q)	$R_{\rm DCO}$(D)	Multipolarity	IPDCO	$J_i^\pi \rightarrow J_f^\pi$
537.5	8386.2	0.5(2)					
550.0	5585.6	<0.5					
550.1	6310.3	0.8(4)					$(\frac{33}{2}^- \rightarrow \frac{31}{2}^-)$
553.2	3441.5	1.0(1)					$\frac{21}{2}^- \rightarrow$
564.7	5035.6	0.7(1)					$\rightarrow \frac{25}{2}$
573.8	6406.1	0.9(1)		0.96(16)	D		$\frac{33}{2}^- \rightarrow \frac{31}{2}^-$
577.8	5760.2	1.0(1)					$(\frac{31}{2}^-) \rightarrow \frac{29}{2}^-$
588.5	8199.3	0.4(1)					$(\frac{39}{2}^- \rightarrow \frac{37}{2}^-)$
596.5	8982.7	<0.5					
611.6	4650.2	25.4(3)	0.59(2)	0.98(4)	$M1$	−0.32(8)	$\frac{27}{2}^- \rightarrow \frac{25}{2}^-$
618.7	4470.9	1.8(1)		1.05(14)	D		$\frac{25}{2} \rightarrow \frac{23}{2}^-$
647.3	3441.5	1.7(2)					$\frac{21}{2}^- \rightarrow \frac{21}{2}^+$
649.9	5832.3	3.0(2)		1.00(17)	$M1$	−0.49(35)	$\frac{31}{2}^- \rightarrow \frac{29}{2}^-$
654.9	5305.1	0.8(1)					$\frac{29}{2}^- \rightarrow \frac{27}{2}^-$
659.9	6441.6	6.5(4)	1.13(11)		Q		$(\frac{31}{2} \rightarrow \frac{27}{2})$
660.7	4102.2	2.5(4)					$\frac{23}{2}^{(-)} \rightarrow \frac{21}{2}^-$
663.8	5314.0	4.4(3)	0.50(6)		D		$\frac{29}{2}^- \rightarrow \frac{27}{2}^-$
668.8	7074.9	0.7(1)					$(\frac{35}{2}^-) \rightarrow \frac{33}{2}^-$
677.5	4529.7	3.2(2)		1.03(8)	D		$\frac{25}{2} \rightarrow \frac{23}{2}^-$
700.5	6769.8	3.6(2)		1.06(18)	D		$\frac{35}{2}^- \rightarrow \frac{33}{2}^-$
724.3	4038.6	0.7(2)					$\frac{25}{2}^- \rightarrow \frac{23}{2}^+$
739.7	5042.0	1.5(2)	0.47(11)		D		$(\frac{27}{2} \rightarrow \frac{25}{2})$
742.1	3536.3	1.6(1)					$\frac{21}{2}^- \rightarrow \frac{21}{2}^+$
786.4	7861.3	0.3(1)					$(\frac{37}{2}^- \rightarrow \frac{35}{2}^-)$
790.9	2794.2	23.3(6)	0.62(2)		$M1$	−0.30(12)	$\frac{21}{2}^+ \rightarrow \frac{19}{2}^+$
816.7	2820.0	1.6(3)					$\rightarrow \frac{19}{2}^+$
823.4	7265.0	4.6(3)	0.89(11)		$E2$	0.40(31)	$(\frac{35}{2} \rightarrow \frac{31}{2})$
841.0	7610.8	0.9(1)					$(\frac{37}{2}^-) \rightarrow \frac{35}{2}^-$
851.2	3645.4	8.6(4)	0.47(1)		$E1$	0.36(20)	$\frac{23}{2}^- \rightarrow \frac{21}{2}^+$
863.1	6932.4	0.6(1)					$\rightarrow \frac{33}{2}^-$
890.0	4205.0	1.6(3)					$\rightarrow \frac{23}{2}^+$
906.6	4945.2	3.6(6)	0.45(4)		$M1$	−0.25(42)	$\frac{27}{2}^- \rightarrow \frac{25}{2}^-$
915.0	5565.2	0.7(2)					$\frac{31}{2}^- \rightarrow \frac{27}{2}^-$
932.8	5267.1	1.5(4)				0.67(62)[a]	$(\frac{23}{2} \rightarrow \frac{21}{2})$
935.1	8200.1	2.4(3)			$E2$	0.67(62)[a]	$(\frac{39}{2} \rightarrow \frac{35}{2})$
948.3	3742.5	3.8(1)	0.95(9)		$E2$	0.44(38)	$\frac{25}{2}^+ \rightarrow \frac{21}{2}^+$
1001.5	1001.5	30.1(11)	0.82(1)		$M1$	−0.38(15)	$\frac{11}{2}^+ \rightarrow \frac{9}{2}^+$
1004.8	4650.2	1.5(3)					$\frac{27}{2}^- \rightarrow \frac{23}{2}^-$
1034.8	2888.3	3.8(2)					$\rightarrow \frac{17}{2}^+$
1044.2	4786.7	2.0(5)					$(\frac{29}{2}^+) \rightarrow \frac{25}{2}^+$
1055.0	9255.1	2.4(3)	0.74(20)		Q		$(\frac{43}{2} \rightarrow \frac{39}{2})$
1058.0	3852.2	1.1(1)					$\frac{23}{2}^- \rightarrow \frac{21}{2}^+$
1143.8	5182.4	2.2(3)					$\frac{29}{2}^- \rightarrow \frac{25}{2}^-$
1219.8	10474.9	0.8(2)	0.76(37)		Q		$(\frac{47}{2} \rightarrow \frac{43}{2})$
1262.0	6337.0	0.5(2)					$\rightarrow (\frac{31}{2}^+)$

TABLE I. *(Continued.)*

E_γ (keV)	E_x (keV)	I_γ	R_{DCO}(Q)	R_{DCO}(D)	Multipolarity	IPDCO	$J_i^\pi \rightarrow J_f^\pi$
1279.5	3282.8	1.0(2)					$\frac{19}{2}^- \rightarrow \frac{19}{2}^+$
1311.0	3314.3	3.9(3)	0.95(3)		$E2$	0.70(66)	$\frac{23}{2}^+ \rightarrow \frac{19}{2}^+$
1318.5	7387.8	<0.5					$\frac{35}{2} \rightarrow \frac{33}{2}^-$
1324.5	3185.5	1.2(3)	0.55(16)		D		
1332.0	3185.5	0.9					$\rightarrow \frac{17}{2}^+$
1333.8	6988.4	0.9(4)					$\frac{33}{2} \rightarrow \frac{31}{2}^-$
1333.8	6544.2	1.0(4)					$\frac{31}{2} \rightarrow \frac{29}{2}^-$
1415.0	1415.0	60.9(20)	0.97(2)		$E2$	0.574(99)	$\frac{13}{2}^+ \rightarrow \frac{9}{2}^+$
1423.0	6989.0	<0.5					$\frac{33}{2} \rightarrow \frac{31}{2}^-$
1429.3	3282.8	12.9(3)	0.47(2)		$E1$	0.50(24)	$\frac{19}{2}^- \rightarrow \frac{17}{2}^+$
1438.2	3441.5	19.1(6)	0.51(2)		$E1$	0.30(15)	$\frac{21}{2}^- \rightarrow \frac{19}{2}^+$
1533.0	3536.3	9.2(3)	0.43(2)		$E1$	0.53(26)	$\frac{21}{2}^- \rightarrow \frac{19}{2}^+$
1537.2	7931.8	0.6(1)					$\rightarrow (\frac{35}{2}^-)$
1718.3	3571.8	0.9(3)	0.35(5)		D		$\frac{19}{2}^{(-)} \rightarrow \frac{17}{2}^+$
1748.8	3751.1	1.9(4)	0.40(7)		D		$\frac{21}{2}^{(-)} \rightarrow \frac{19}{2}^+$
2331.0	4334.5	0.6(4)					$(\frac{21}{2}) \rightarrow \frac{19}{2}^+$

[a]Polarization measured for combined (933 + 935)-keV γ transitions.

204-keV transitions. The intensity of the 597-keV transition was found to be equal in the gate of 393- and 612-keV transitions, indicating that it is present elsewhere and not linking the states ($25/2^- \rightarrow 21/2^-$). The 597-keV transition has been placed in band 3. The band was also found to decay to various newly found levels at lower excitation energies. The transitions linking these low lying states were found to be in coincidence with the transitions of the band but not in coincidence with the 1429-keV transition. Besides, the states $21/2^-$ and $19/2^-$ of band 1 were found to be fed from the states $23/2^-$ and $21/2^-$ of band 2 via the transitions of energy 411 and 253 keV, respectively.

2. Band 2

The band has been observed in earlier works [5,8]. In the present work, the intensities of transitions of the band are found

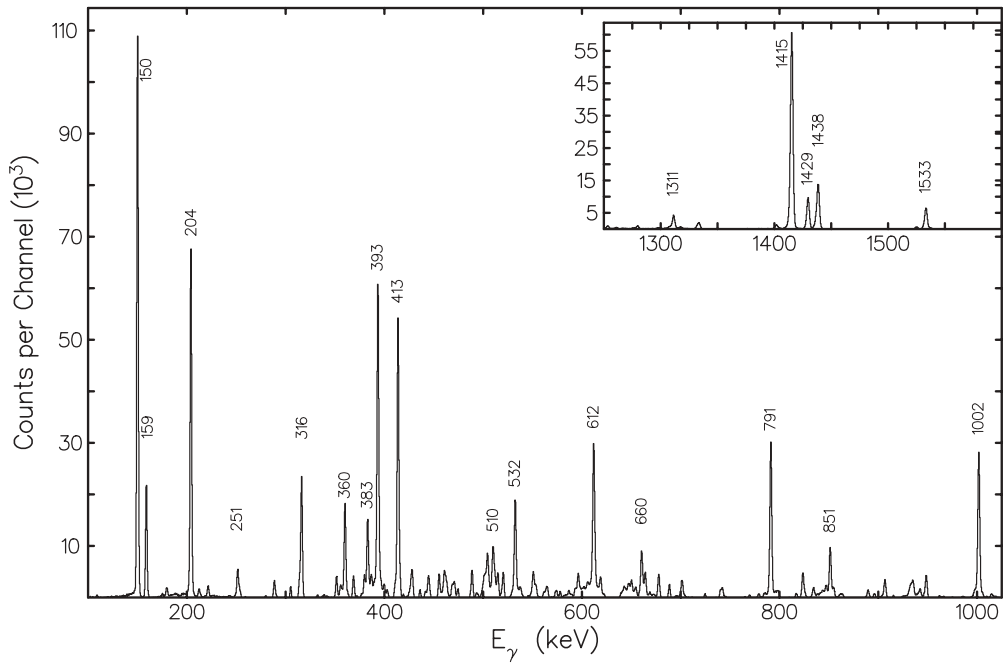

FIG. 3. γ-ray coincidence spectrum with a gate set on the 438-keV transition of ^{107}In. The inset shows the higher energy part of the spectrum.

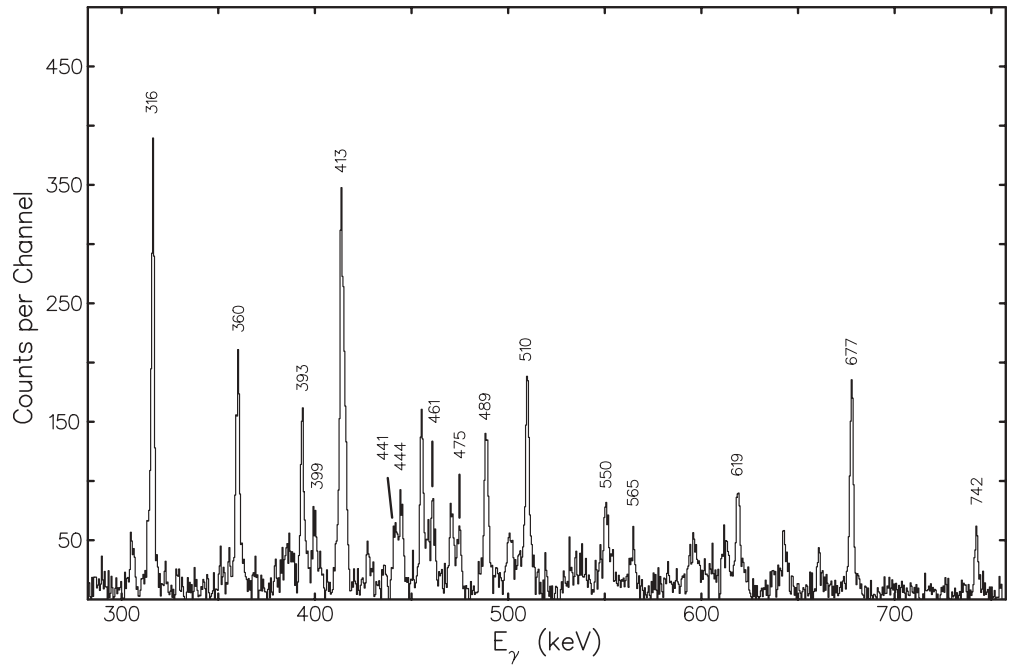

FIG. 4. Sum double-gated γ-ray coincidence spectrum with the first gate on the 438-keV transition and the second gate on the 316-, 360-, and 1533-keV transitions of ^{107}In.

to be significantly less than reported in earlier works. The γ-ray intensities of all the transitions above the 3852-keV level of the band were measured using two different coincidence gates. In the first case the gate was set on the 1415-keV transition and intensities were normalized with respect to the 438-keV transition. In the second case the gate was set on 1533 keV and the normalization of intensities was done with respect to the 316-keV transition. On comparison, we observed that the intensities of 444-, 488-, 510-, and 360-keV transitions deduced from the 1533-keV gate were significantly less than those deduced from the 1415-keV gate. This indicates the presence of these transitions somewhere else in the level scheme also. The relative placement as suggested by their intensity profile is the same as reported earlier [5,8]. The 360-keV transition is subsequently placed also in band 6. The other change includes the placement of another 1334-keV

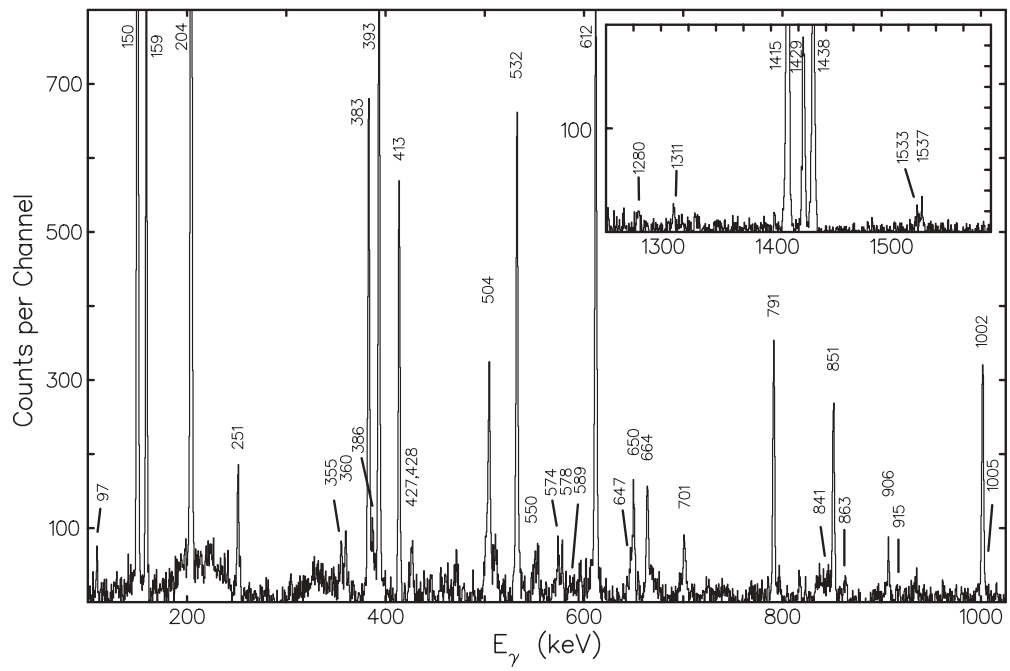

FIG. 5. Sum double-gated γ-ray coincidence spectrum with the first gate on the 438-keV transition and the second gate on the 393-, 612-, and 532-keV transitions of ^{107}In. The inset shows the higher energy part of the spectrum.

transition feeding the band from the top at the $29/2^-$ level. The intensity of the 1334-keV transition in the gate of 1533 keV was observed to be quite large as compared with the observed intensity of the 444-keV transition in the same gate. Further, the intensities of the 1334-keV transition were compared in the coincidence spectrum gated by the 444- and 488-keV transitions, respectively. It was found that the intensity of this transition observed in the gate of the 488-keV transition was almost double the intensity observed in the gate of the 444-keV transition. This leads to the conclusion of having two 1334-keV transitions with nearly equal energies, one of them feeding the band at 5655 keV and the other at 5210 keV. The DCO ratio and polarization measurements confirmed the multipole character of the 316-keV transition to be $M1$ and that of the 1533-keV transition to be $E1$. This establishes $I^\pi = 21/2^-$ and $23/2^-$ for the 3536- and 3852-keV levels, respectively. The 360-, 510-, 488-, and 444-keV transitions were determined as dipoles from the DCO ratio measurements. This helped in the assigned I^π values (see Fig. 2) for band 2.

3. Band 3

The sequence of transitions of energies 399, 460, 537, and 596 keV was found in coincidence with the transitions of band 2 and the 1334-keV transition and these transitions are grouped as band 3. The relative intensities as calculated from the 1533-keV gate suggested the placement as shown in the level scheme (see Fig. 2). The DCO ratio determined the dipole nature of the 399-keV transition. The band also decays via another path to band 2. Band 3 was also found to decay to the levels at 6069 and 5566 keV in band 1 via 1319- and 1423-keV transitions from the levels at 7388 and 6989 keV, respectively.

4. Bands 4, 5, 6, and 7

A series of bands labeled as bands 4, 5, 6 and 7 was also observed in this study. Band 4 consists of 574-, 669-, and 786-keV transitions with a linking transition of energy 650 keV to the $29/2^-$ level of band 1. Band 5 consists of 355-, 471-, and 1537-keV transitions and a tentative 586-keV transition. The band was found to be linked to band 1 at the $29/2^-$ level via a 386-keV transition. Band 6 consists of transitions of energies 360, 455, and 550 keV, with a linking transition of 907 keV connecting band 6 to band 1 at the $25/2^-$ level. The placement of all the transitions of bands 4, 5, and 6 was based on the γ-ray intensities determined from the spectrum gated on the 393-keV transition. Since a pair of coincident transitions of energies 392 and 905 keV is also present in ^{105}Cd, being also populated in the same reaction, the relative placement of the 907- and 360-keV transitions was done on the basis of intensities determined from the double-gated spectrum with gates on the 438- and 393-keV transitions. The placement of transitions in bands 4, 5, and 6 was also confirmed via alternative gates. For example, in the gate of the 383-keV transition, the transitions of bands 4, 5, and 6 were not observed. For band 6, the 907-keV transition was not observed in the gate of the 612-keV transition. Other transitions of band 6 were found to have lower intensities in the gate of the 612-keV transition in comparison to the intensities determined from the gate of the 393-keV transition. The DCO ratio and polarization measurements of the linking transitions (at 386, 650, and 907 keV) establishes their $M1$ character. Further, the DCO ratios of in-band transitions of bands 4, 5, and 6 determined their dipole nature. The spin and parity assignment in these bands were based on these measurements.

Band 7 has been reported in an earlier study [8]. The only change made in the present work was the placement of the 428-keV transition, which was found to connect the 3743- and 3315-keV levels, and the addition of 402- and 1262-keV transitions at the top of the band as shown in Fig. 2. The nature of the 948-keV transition has been found to be $E2$ from the DCO ratio and polarization measurements. This new result establishes $I^\pi = 25/2^+$ for the 3742-keV level.

5. Band 8

The sum double-gated γ-ray coincidence spectrum for band 8 is shown in Fig. 6. A sequence of transitions of energies 515, 660, 823, 935, 1055, and 1220 keV in coincidence with each other was observed. The placement of transitions above the 660-keV transition was based on the γ-ray intensities obtained in the double-gated spectrum of 660- and 438-keV transitions. The transitions of the band have also been found in coincidence with 933- and 2331-keV transitions. A loss of intensity at the 5782-keV level was observed in the gate of the 823-keV transition. Subsequently, a decay transition of energy 740 keV was found from the 5782-keV level on the basis of coincidence results. For obtaining the intensities of transitions of the band, first the intensities of 515- and 823-keV transitions were obtained in the gate of the 1415-keV transition then the intensities of the remaining transitions were obtained in the gate of the 515-keV transition, with normalization done with respect to the intensity of the 823-keV transition obtained in the same gate. The 823-keV transition was used to scale the intensities of other transitions of the band because of the neighboring transitions in the 660-keV region. The band has also been recently reported in the work of Refs. [9,10]. In the work of Ref. [10], the band has been extended with the addition of 1389-, 1573-, and 1789-keV transitions and a tentative 1970-keV transition along with a decay transition of energy 1527 keV from the 5265-keV level and a tentative linking transition of energy 594 keV (4333 to 3739 keV). These transitions were not observed in the present work. The DCO ratios of the in-band transitions agree with their quadrupole nature. In addition, from the polarization measurements, the 823-keV and the combined (933 + 935)-keV transitions were determined to be of electric character. Thus the in-band transitions of the band were confirmed to be of $E2$ nature.

B. Lifetime measurement

Lifetimes of the states of band 1 and band 8 have been measured by the Doppler-shift attenuation method (DSAM). For the DSAM analysis of band 1, asymmetric DCO- matrices as described in Sec. II were used. Out of the four angle-dependent matrices made, two of these were used, the 148° versus 90° matrix for backward line-shape analysis and the 32° versus 90° matrix for forward line-shape analysis. The choice of keeping 90° detectors on one axis rather than keeping all detectors was made so that a gate on a complete peak could be set. This is necessary if the gating transitions have

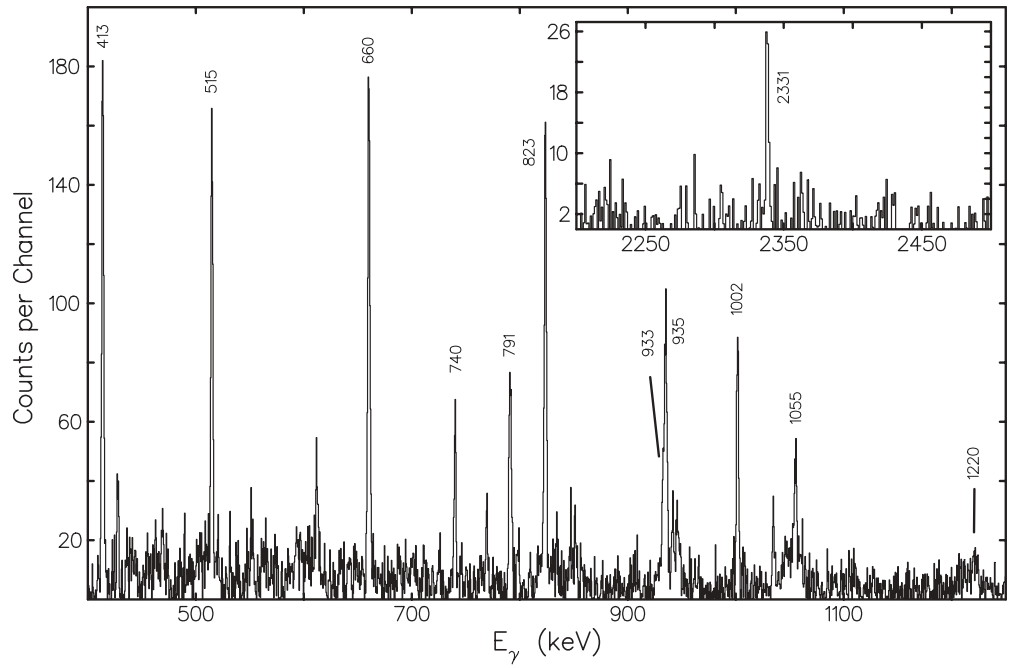

FIG. 6. Sum double-gated γ-ray coincidence spectrum with the first gate on the 438-keV transition and the second gate on the 660-, 823-, 933-, and 935-keV transitions of ^{107}In. The inset shows the higher energy part of the spectrum.

Doppler-shifted counts. In the analysis the gating transitions were always below the transition of interest. For the DSAM analysis of band 8, 148° versus and 32° versus all matrices were used as this provided line shapes with better statistics compared with the matrix format used for band 1 line-shape analysis. And since the spectra were made with gates set on 660- and 823-keV transitions, which were observed to have no Doppler shift, it was possible to have a gate on a complete peak while gating on the "all" axis. For line-shape analysis of the transitions the LINESHAPE program [21] was used. The program takes into account the energy loss of the beam through the target and the energy loss and angular straggling of the recoils through the target and the backing. For the stopping power option we used the shell-corrected Northcliffe and Schilling stopping powers [22]. The value of the time step and the number of recoil histories were chosen to be 0.001 ps and 5000, respectively.

In band 1, the Doppler-broadened line shapes were observed for transitions above the 3442-keV $21/2^-$ state. In the analysis, the lifetimes of individual levels of the band were obtained. The crossover $E2$ transitions were included as a part of side feeding to the corresponding populating state. The side feeding into each level has been modeled first as a single-step feeding, which then was later changed to rotational feeding once a suitable set of window and transition parameters was achieved. The side-feeding times were found to be an order of magnitude smaller than the level lifetimes. The rotational feeding of the states has therefore been assumed. Fitting was started at the top level with all the parameters of other levels kept fixed. Once the χ^2 minimization was achieved by the MINUIT program, the background and the contaminant peak parameters were fixed and the procedure was followed for the next lower level. After obtaining χ^2 minimization for each level, a global fit was carried out, with the background and the contaminant peak parameters of all the levels kept fixed. The results are listed in Table II and the fitting of the theoretical line shape with the experimental data for 393- and

TABLE II. Lifetimes of states and reduced $M1$ strengths of transitions of band 1 of ^{107}In. The systematic errors from the uncertainty in stopping powers (∼15%) are not included in the results.

I_i^π	$E_{\gamma,M1}$ (keV)	$E_{\gamma,E2}$ (keV)	τ (ps)	$B(M1)$ $(\mu_N)^2$	$B(E2)$ $(e\ \mathrm{b})^2$	$B(M1)/B(E2)$ $(\mu_N/e\ \mathrm{b})^2$
$\frac{23}{2}^-$	203.9		$1.56^{+0.17}_{-0.16}$	$3.24^{+0.37}_{-0.33}$		
$\frac{25}{2}^-$	393.2		$0.64^{+0.01}_{-0.02}$	$1.44^{+0.07}_{-0.07}$		
$\frac{27}{2}^-$	611.6	1004.8	$0.72^{+0.02}_{-0.03}$	$0.33^{+0.02}_{-0.01}$	$0.0043^{+0.0009}_{-0.0007}$	$76.7^{+13.3}_{-18.0}$
$\frac{29}{2}^-$	532.2	1143.8	$0.65^{+0.02}_{-0.02}$	$0.51^{+0.03}_{-0.04}$	$0.0058^{+0.0010}_{-0.0007}$	$87.9^{+11.8}_{-15.3}$
$\frac{31}{2}^-$	382.8	915.0	$0.76^{+0.04}_{-0.03}$	$1.02^{+0.09}_{-0.06}$	$0.0069^{+0.0028}_{-0.0016}$	$147.8^{+36.7}_{-60.6}$
$\frac{33}{2}^-$	504.1		$0.53^{+0.02}_{-0.02}$	$0.84^{+0.03}_{-0.03}$		
$\frac{35}{2}^-$	700.5		$0.43^{+0.03}_{-0.03}$[a]	$0.38^{+0.03}_{-0.02}$		

[a]Effective lifetime.

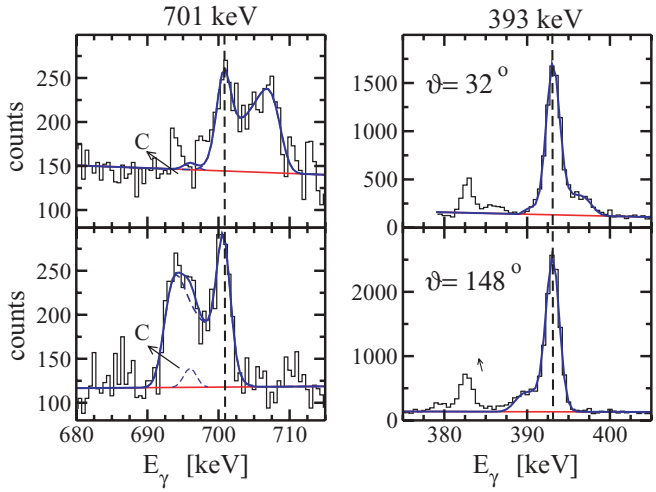

FIG. 7. (Color online) Experimental and theoretical line shapes of transitions of band 1. Top and bottom figures correspond to forward and backward spectra, respectively. Contaminant peaks are labeled as C with the dashed curve depicting their shape.

701-keV transitions is shown in Fig. 7. The errors quoted in lifetimes does not include the systematic errors from the uncertainty in stopping power, which can be as large as 15%. Also listed in the table are the experimental $B(M1)$ and $B(E2)$ values deduced from the level lifetimes τ using the following relationships [23]:

$$B(M1) = \frac{0.05697 B_\gamma(M1)}{E_\gamma^3(M1)\tau[1+\alpha_t(M1)]}\left[\mu_N^2\right] \quad (4)$$

and

$$B(E2) = \frac{0.0816 B_\gamma(E2)}{E_\gamma^5(E2)\tau[1+\alpha_t(E2)]}[(e\ \mathrm{b})^2], \quad (5)$$

where B_γ and α_t are the branching ratio and the total internal conversion coefficient of the transition, respectively.

In band 8, line shapes were observed in 935-, 1055-, and 1220-keV transitions. To have better statistics for the line-shape analysis of the 1220-keV transition, the sum of spectra with gates on 660- and 823-keV transitions were used, whereas for the line-shape analysis of 1055-keV transition it was sufficient to have a spectrum with a gate on the 660-keV transition. Owing to the presence of the 658- and 932-keV coincident pair of transitions coming from ^{104}Cd, also populated in the reaction, the spectrum with the gate on the 660-keV transition cannot be used for the line-shape analysis of the 935-keV transition. Instead, the gate on the 823-keV transition provided a clean spectrum for the line-shape analysis of the 935-keV transition. The fittings of the theoretical line shapes with the data for 1055-, 1220-, and 935-keV transitions are shown in Fig. 8. The side-feeding lifetimes were found to be an order of magnitude less than the corresponding level lifetimes. From the measured $B(E2)$ strengths, transition quadrupole moments Q_t were obtained using the following expression [23]:

$$B(E2, I_i K \rightarrow I_f K) = \frac{5}{16\pi}\langle I_i K 20 | I_f K\rangle^2 e^2 Q_t^2. \quad (6)$$

For the states under consideration it is reasonable to assume $I \gg K$ while determining Q_t using this equation. We also assume that the nucleus is axially symmetric at these spins and calculated the deformation β_2 by the following expression [24]:

$$Q_t = \frac{3}{\sqrt{5\pi}} Z R_\circ^2 A^{2/3}\beta_2(1+0.36\beta_2). \quad (7)$$

The results for the band are listed in Table III and do not include the systematic errors from the uncertainty in stopping powers ($\sim \pm 15\%$).

IV. DISCUSSION

In the discussion that follows, the experimental data are compared with the predictions of TAC model calculations.

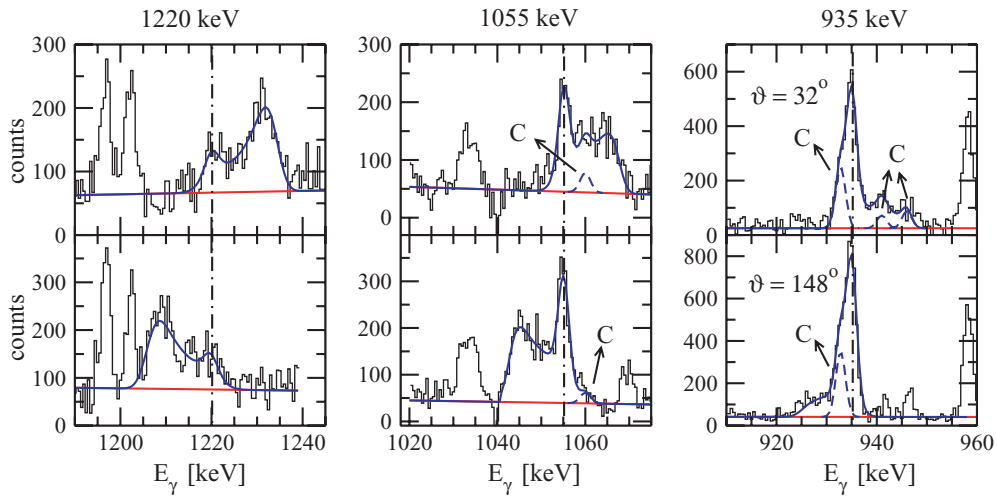

FIG. 8. (Color online) Experimental and theoretical line shapes of transitions of band 8. Top and bottom figures correspond to forward and backward spectra, respectively. Contaminant peaks are labeled as C with the dashed curve depicting their shape.

TABLE III. Lifetimes of states and reduced $E2$ strengths of transitions of band 8 of ^{107}In. The systematic errors from the uncertainty in stopping powers (∼15%) are not included in the results.

I_i^π	E_γ (keV)	τ (ps)	$B(E2)$ $(e\,\mathrm{b})^2$	Q_t (e b)	β_2
$\frac{39}{2}$	935.1	$0.43^{+0.02}_{-0.02}$	$0.27^{+0.01}_{-0.02}$	$2.69^{+0.12}_{-0.15}$	0.21
$\frac{43}{2}$	1055.0	$0.35^{+0.01}_{-0.01}$	$0.18^{+0.01}_{-0.01}$	$2.19^{+0.12}_{-0.12}$	0.17
$\frac{47}{2}$	1219.8	$0.24^{+0.01}_{-0.01}$ [a]	$0.13^{+0.01}_{-0.01}$	$1.86^{+0.14}_{-0.14}$	0.15

[a]Effective lifetime.

The values of the proton paring gap parameter $\Delta_\pi = 0.99$ and the neutron pairing gap parameter $\Delta_\nu = 0.85$ were used in the TAC calculations. These values are 0.6 and 0.8 times the odd and even mass difference, respectively. The chemical potential λ_ν was chosen so that a particle number of $N = 58$ is reproduced. The values of deformation parameter ϵ_2 and γ were obtained by Nilsson Strutinsky's minimization procedure [25]. The nature of band 2, which is a $\Delta I = 1$ negative-parity $M1$ band, could not be determined. Although it appears to be an aligned band, no configuration has been assigned to it.

A. Band 1

The linear polarization measurements for the decay and in-band transitions have confirmed that band 1 is a $\Delta I = 1$, $M1$, negative-parity band. In the isotone ^{105}Ag, a similar negative-parity band (band 3 of Ref. [2]) has been observed and was assigned the $\pi(g_{9/2}) \otimes \nu[(h_{11/2})(d_{5/2}/g_{7/2})]$ configuration. In Fig. 9 the observed spins I of band 1 of ^{105}In [5] and ^{107}In (present work) as a function of rotational frequency $\omega(I)$ are plotted. For comparison, a similar plot for the negative-parity bands (band 1 and band 2) of ^{108}In [26] is also shown. These bands of ^{108}In have a $\pi(g_{9/2})^{-1} \otimes \nu(h_{11/2})$ configuration before the alignment (band 1) and a $\pi(g_{9/2})^{-1} \otimes \nu[h_{11/2}(d_{5/2}/g_{7/2})^2]$ configuration after the alignment (band 2). The band-crossing frequency of the

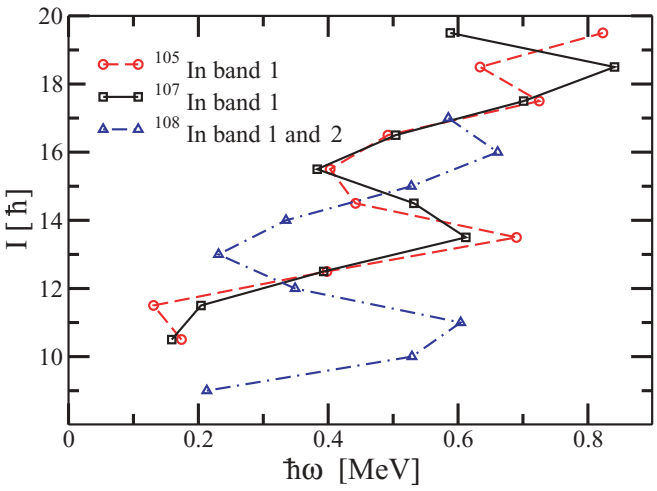

FIG. 9. (Color online) Angular momentum as a function of rotational frequency for band 1 in ^{105,107}In and bands 1 and 2 in ^{108}In [26].

$(d_{5/2}/g_{7/2})$ aligned neutron pair is about 0.40 MeV and the alignment gain is about $5\hbar$. In ^{105}In and ^{107}In the alignment frequency is about 0.43 MeV and the alignment gain is about $4.5\hbar$. The similar behavior of the plots for ^{105}In, ^{107}In, and ^{108}In show the involvement of the same pair of neutrons, namely $(d_{5/2}/g_{7/2})^2$, in the rotational alignments in these bands. Based on these arguments, we suggest that band 1 of ^{107}In has a three-quasiparticle $\pi(g_{9/2})^{-1} \otimes \nu[h_{11/2}(d_{5/2}/g_{7/2})]$ configuration before the alignment and a five-quasiparticle $\pi(g_{9/2})^{-1} \otimes \nu[h_{11/2}(d_{5/2}/g_{7/2})^3]$ configuration after the alignment.

The experimental results of band 1 of ^{107}In are compared with TAC calculations done for the configurations mentioned in previous paragraph. In the calculations, static deformations of $\epsilon_2 = 0.12$, $\gamma = 15^\circ$ and $\epsilon_2 = 0.13$, $\gamma = 10^\circ$ for configurations before and after the alignment, respectively, are used. The results of calculations for the $I(\omega)$ curve are shown in Fig. 10, where a good agreement between the theoretical calculations and the experimental results is obtained. The experimental $B(M1)$ strengths, deduced from measured lifetimes, as a function of spin I are plotted in Fig. 11, along with the $B(M1)$ strengths calculated from the TAC calculations. The experimental data on $B(M1)$ values, particularly its sharp decrease with increasing spin before the alignment of neutrons, indicate that the deformation of the core for these multiparticle configurations would be quite less than the value obtained from Strutinsky's minimization procedure. The calculations are therefore also performed with a lower value of deformation parameter (i.e., $\epsilon_2 = 0.08$) obtained by reducing the strength of the coupling constant of the quadrupole-quadrupole (QQ) interaction. Using this low value of ϵ_2, we see from Fig. 10 and Fig. 11 that a better agreement of calculations with

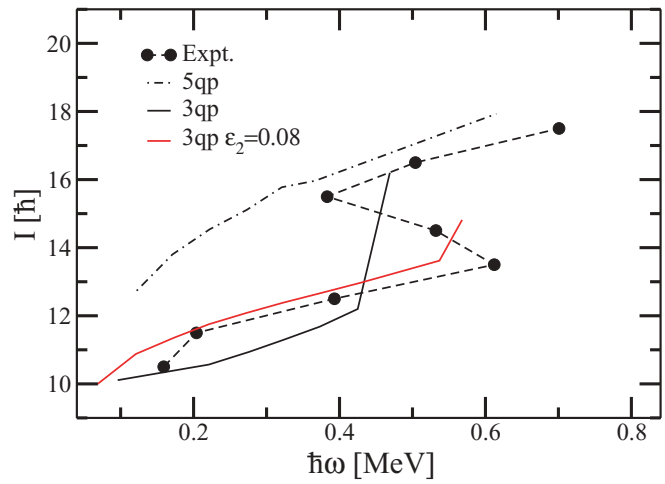

FIG. 10. (Color online) Angular momentum as a function of rotational frequency for band 1 in ^{107}In. Comparison with TAC calculations are shown. 3qp stands for calculations for the three-quasiparticle configuration $\pi(g_{9/2})^{-1} \otimes \nu[h_{11/2}, (d_{7/2}/g_{7/2})]$ of the band before the alignment. Similarly, 5qp stands for calculations for the five-quasiparticle configuration $\pi(g_{9/2})^{-1} \otimes \nu[h_{11/2}, (d_{7/2}/g_{7/2})^3]$ of the band after the alignment. Also shown are the calculations done with the lower deformation value of $\epsilon_2 = 0.08$ for the 3qp configuration.

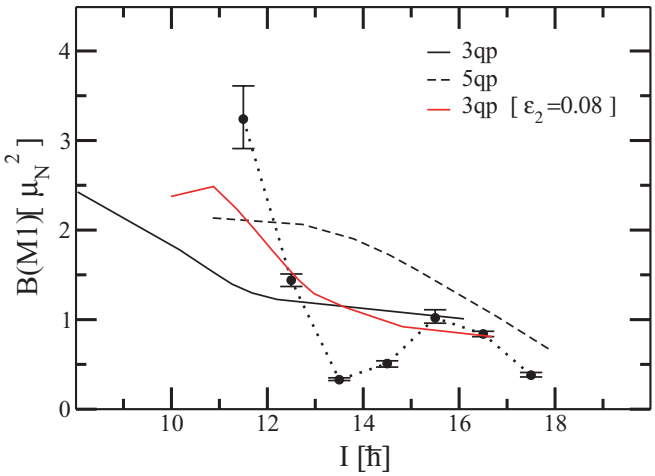

FIG. 11. (Color online) Experimental $B(M1)$ strengths as a function of spin for band 1 in ^{107}In. Comparison with TAC calculations are shown. Calculations done with a lower value of deformation parameter $\epsilon_2 = 0.08$ for the 3qp configuration are also compared.

experimental results before the alignment is obtained. A similar situation has been observed in the case of band 1 of ^{106,108}Sn [27,28], where the states have lower deformation than obtained through the minimization procedure. The low deformation of these states indicates that the contribution from the core in spin generation is negligible and the whole of the spin generation along the band can be attributed to the shears mechanism. The decrease in $B(M1)$ values (Fig. 11) with increase in spin both before and after the alignment establishes the shears mechanism as the dominant contribution in the generation of spin for this sequence of states.

B. Band 8

The in-band transitions in band 8 have been determined to be of $E2$ character. From the measured $B(E2)$ strengths, the deformation of the band is found to have $\beta_2 \sim 0.2$. Similar deformed bands have been observed in this mass region [29–31] and are associated with the phenomenon of smooth band termination (STB) [32]. The Crank-Nilsson-Strutinsky (CNS) calculations for the band have been carried out by Ideguchi *et al.* [10]. The $\pi[(g_{9/2})^{-2}(d_{5/2}/g_{7/2})] \otimes \nu[(h_{11/2})^2(d_{5/2}/g_{7/2})^6]$ configuration has been suggested. The decreasing β_2 value (see Table III) is consistent with the change of nuclear shape from prolate to oblate.

V. CONCLUSION

The level scheme of ^{107}In has been extended considerably with the observation of several $\Delta I = 1$ bands and one $\Delta I = 2$ band. Deduced $B(M1)$ strengths for band 1 before the alignment has established the shears mechanism as the dominant mode of angular momentum generation with almost no contribution from the core. These states are an example of good magnetic rotors. Such an example has also been found in ^{106}Sn and to some extent in ^{108}Sn. These results indicate that nuclei close to the doubly magic ^{100}Sn, having very low deformation, need to be investigated to gain new insights into these structures. It may be mentioned that the TAC model inherently requires a deformed mean field to describe such states. Band 8 has been identified as a deformed band with deformation $\beta_2 \sim 0.2$. However, for the high spin states reported in [10], lifetime measurements will be useful to understand the evolution of collectivity within the band.

ACKNOWLEDGMENTS

We would like to thank the operational staff of the 15UD Pelletron at IUAC and the INGA Collaboration. Thanks are also due to the target laboratory, IUAC, New Delhi. Sincere thanks are offered to Prof. A. Macchiavelli and Dr. S. Ray for helpful discussions. One of the authors (D.N.) would like to acknowledge the financial assistance in the form of a fellowship from the Council of Scientific and Industrial Research (CSIR), India. The authors would like to thank the Department of Science and Technology, Government of India, for providing funding for the INGA project (No. IR/S2/PF-03/2003-I).

[1] S. Frauendorf, Rev. Mod. Phys. **73**, 463 (2001).
[2] A. Deo *et al.*, Phys. Rev. C **73**, 034313 (2006).
[3] P. Vaska *et al.*, Phys. Rev. C **57**, 1634 (1998).
[4] A. Deo *et al.*, Phys. Rev. C **79**, 067304 (2009).
[5] J. Kownacki *et al.*, Nucl. Phys. A **627**, 239 (1997).
[6] E. Andersson, P. Herges, H. V. Klapdor, and I. N. Wischnewski, Phys. Rev. C **24**, 917 (1981).
[7] D. Kast *et al.*, Eur. Phys. J. A **3**, 115 (1998).
[8] S. K. Tandel, S. B. Patel, P. Joshi, G. Mukherjee, R. P. Singh, S. Muralithar, P. Das, and R. K. Bhowmik, Phys. Rev. C **58**, 3738 (1998).
[9] S. Sihotra, Z. Naik, R. Palit, A. Y. Deo, S. Kumar, P. K. Joshi, D. Mehta, and N. Singh, Eur. Phys. J. A **43**, 45 (2010).
[10] E. Ideguchi *et al.*, Phys. Rev. C **81**, 034303 (2010).
[11] G. K. Mehta and A. P. Patro, Nucl. Instrum. Methods Phys. Res. **268**, 334 (1988).
[12] B. P. Ajith Kumar, J. Kannaiyan, P. Sugathan, and R. K. Bhowmik, Nucl. Instrum. Methods A **343**, 327 (1994).
[13] R. K. Bhowmik, in *Proceedings of Fourth International Conference on Fission and Properties of Neutron-Rich Nuclei, 2007,* edited by J. H. Hamilton, A. V. Ramayya, and H. K. Carter (World Scientific, Singapore, 2008), pp. 258–263.
[14] S. Muralithar *et al.* (Communicated to Nucl. Instr. Methods A).
[15] B. P. Ajith Kumar, E. T. Subramanium, K. M. Jayan, S. Mukherjee, and R. K. Bhowmik, in *Proceedings on the Symposium on Advances in Nuclear and Allied Instruments, India, 1997* (Tata McGraw-Hill, New Delhi, 1997), pp. 51–55.
[16] R. K. Bhowmik, S. Muralithar, and R. P. Singh, *Proceedings of the DAE-BRNS Symposium on Nuclear Physics*, Vol. B44, p. 422 (India, 2001).
[17] D. C. Radford, Nucl. Instrum. Methods A **361**, 297 (1995).

[18] M. K. Kabadiyski, K. P. Lieb, and D. Rudolph, Nucl. Phys. A **563**, 301 (1993).
[19] K. Starosta *et al.*, Nucl. Instrum. Methods A **423**, 16 (1999).
[20] R. Palit, H. C. Jain, P. K. Joshi, S. Nagaraj, B. V. T. Rao, S. N. Chintalapudi, and S. S. Ghugre, Pramana **54**, 347 (2000).
[21] J. C. Wells, ORNL Physics Division Progress, Report No. ORNL-6689, September 30, 1991.
[22] L. C. Northcliffe and R. F. Schilling, Nucl. Data. Tables A **7**, 233 (1970).
[23] H. Ejiri and M. J. A. de Voigt, *Gamma-Ray and Electron Spectroscopy in Nuclear Physics* (Clerendon, Oxford, 1989), Chapter 6.
[24] N. R. Johnson *et al.*, Nucl. Phys. A **557**, 347c (1993).
[25] V. Strutinsky, Nucl. Phys. A **95**, 420 (1967).
[26] C. J. Chiara *et al.*, Phys. Rev. C **64**, 054314 (2001).
[27] D. G. Jenkins *et al.*, Phys. Lett. B **428**, 23 (1998).
[28] D. G. Jenkins *et al.*, Phys. Rev. Lett. **83**, 500 (1999).
[29] H. Schnare *et al.*, Phys. Rev. C **54**, 1598 (1996).
[30] R. Wadsworth *et al.*, Phys. Rev. Lett. **80**, 1174 (1998).
[31] E. S. Paul *et al.*, Phys. Rev. C **76**, 034323 (2007).
[32] I. Ragnarsson, V. P. Janzen, D. B. Fossan, N. C. Schmeing, and R. Wadsworth, Phys. Rev. Lett. **74**, 3935 (1995).